Scientific Visualization, 2025, volume 17, number 1, pages 45 - 64, DOI: 10.26583/sv.17.1.05

3D-Cloning of Core Plug Structures: Insights and Challenges into FDM and DLP Printing Based on Microtomography Data

R. I. Kadyrov[1,A], T. H. Nguyen[2,A], E. O. Statsenko[3,A], N.V. Kharin[4,B]

[A] Kazan Federal University (Institute of Geology and Petroleum Technologies), Kazan, Russia
[B] Kazan Federal University (Institute of Mathematics and Mechanics), Kazan, Russia

[1] ORCID: 0000-0002-7566-6312, rail7777@gmail.com
[2] ORCID: 0000-0001-6155-9017, thanhtu154@gmail.com
[3] ORCID: 0000-0001-6259-1713, e.statsenko@yahoo.com
[4] ORCID: 0000-0003-4850-143X, nik1314@mail.ru

Abstract

This study explores the use of FDM (Fused Deposition Modeling) and DLP (Digital Light Processing) 3D printing techniques to create accurate replicas of core plugs from reservoir rock structures based on μCT (microtomography) scans. Due to the challenges in obtaining core plug samples for reservoir characterization, this research aims to develop a cost-effective and reusable alternative by replicating the pore structure of natural rocks for use in experimental studies. A carbonate core plug was μCT-scanned to obtain a high-resolution 3D digital model of its pore structure, which was then digitally processed to simplify its complex pore geometry for 3D printing. The model was printed using FDM with 0.2 mm and 0.4 mm nozzles, as well as DLP techniques. Both methods were evaluated by re-scanning the printed samples with μCT and analyzing their structural, porosity, and permeability characteristics. FDM printing demonstrated the ability to replicate larger pore structures, but the presence of interlayer gaps resulted in inflated porosity and permeability values compared to the original core plug, and fine pore features were inconsistently replicated across multiple prints. DLP printing, while more accurate in capturing morphology and finer details, also exhibited variability in the reproduction of small pore elements. Furthermore, cracks were observed in DLP samples due to stresses during resin curing, and the retention of residual resin in pores affected permeability and reduced effective porosity. The study highlights the limitations of both FDM and DLP methods in fully reproducing the complexity of pore networks, particularly at fine scales. The results point to the need for technological improvements in both methods to enhance the accuracy and reproducibility of 3D-printed core replicas.

Keywords: 3D-cloning, replication, core plug, reservoir, porous structure, μCT, 3D-printing, FDM, DLP.

1. Introduction

The oil & gas industry worldwide is rapidly evolving and searching for more efficient and economical exploration and extraction methods, which increases the need for extensive reservoir studies [1,2]. Standard core plugs play a pivotal role in this domain, serving as representative models of subsurface geological formations where petroleum and gas deposits are found [3,4]. These reservoir samples serve as invaluable tools for scientists and engineers, providing critical insights into the physical and chemical properties of rocks and fluids deep beneath the Earth's surface. Understanding these properties is essential for predicting oil and gas reservoir behavior, optimizing extraction techniques, and ensuring efficient and sustainable resource exploitation [5].

Extracting core samples is a costly and time-consuming process, often requiring advanced drilling techniques and specialized equipment. Moreover, accessing certain reservoirs, especially those located in remote or environmentally sensitive areas, can be logistically challenging. These factors limit the quantity and variety of core samples available for analysis, constraining the scope of research and potentially hindering comprehensive understanding of reservoir characteristics [3].

In addition, a significant limitation arises from the inability to reuse samples after a series of tests due to contamination and sample destruction. Each experimental procedure, particularly those involving chemical interaction or mechanical testing, can alter the composition and physical integrity of the core samples, rendering them unsuitable for subsequent tests. This restriction poses a challenge in conducting a diverse range of experiments on a limited set of core samples, necessitating an ongoing need for fresh samples from drilling operations [6].

Moreover, an often-underestimated limitation in core analysis stems from the inherent variability in the pore structure of core samples, even when they share similar compositions and properties. Despite their similar geological origins, these samples exhibit diverse pore network architectures, impacting the results of experiments. The influence of pore structure on fluid flow, mechanical behaviour, and chemical interactions is substantial but frequently overlooked. This variation becomes particularly critical when testing methods aimed at enhancing oil recovery or studying the effects of different chemical compositions. Variations in the pore structure can significantly skew experimental outcomes, leading to inaccurate interpretations and potentially flawed conclusions [6].

In the face of these limitations in core analysis, the prospect of creating clones of standard core plugs replicating the pore space structure through 3D printing technology sparks significant interest within the scientific community [7,8]. All 3D printers operate on a fundamental principle – the layer-by-layer construction of objects using thin horizontal slices of material. These methods are broadly categorized based on the type of material used and the way the material is layered or solidified to create objects [9] (Fig. 1).

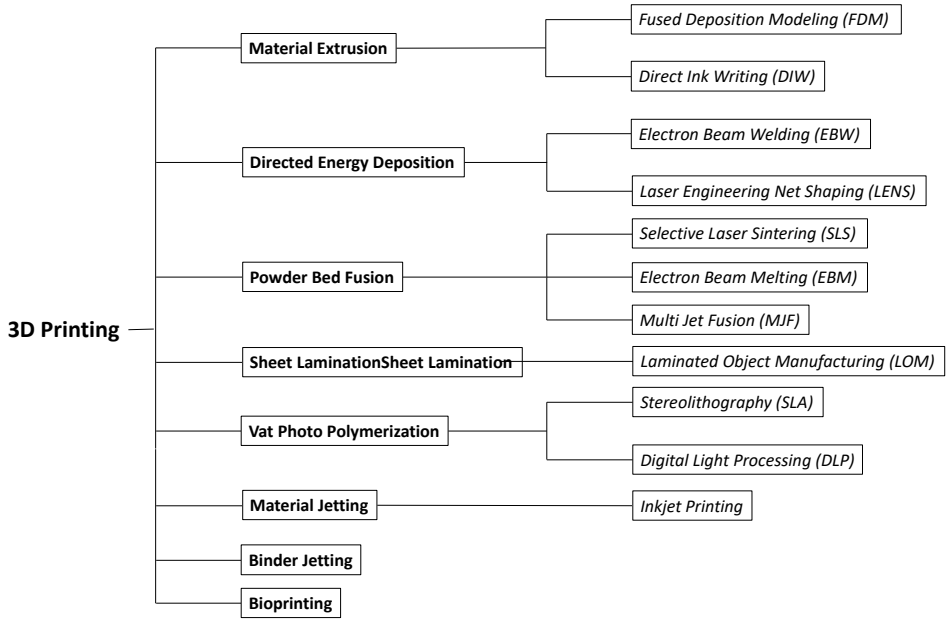

Fig. 1. Classification of 3D printing methods

Material Extrusion involves extruding material through a nozzle to build objects layer by layer. The two main techniques are *Fused Deposition Modeling (FDM)*, which uses thermoplastic filaments, and *Direct Ink Writing (DIW),* which can use a variety of materials, including pastes and gels.

Directed Energy Deposition (DED) uses focused thermal energy to fuse materials as they are being deposited. Techniques under this category include *Electron Beam Welding (EBW),* which uses an electron beam, and *Laser Engineering Net Shaping (LENS),* which uses a laser to melt metal powder or wire.

Powder Bed Fusion (PBF) involves using a heat source to fuse powder particles together layer by layer. *Selective Laser Sintering (SLS)* uses a laser to sinter polymer powder, while *Electron Beam Melting (EBM)* uses an electron beam to melt metal powder, creating dense metal parts. *Multi Jet Fusion (MJF)* is another method within this category that uses an inkjet array to apply fusing agents on a powder bed, followed by a thermal process to fuse the powder.

Sheet Lamination builds objects by stacking and bonding sheets of material. *Laminated Object Manufacturing (LOM)* is a key technique, where layers of adhesive-coated paper, plastic, or metal laminates are bonded together and cut to shape.

Vat Photo Polymerization uses a vat of liquid photopolymer resin cured by a light source to form solid objects layer by layer. *Stereolithography (SLA)* is a well-known method that employs a UV laser to cure the resin. *Digital Light Processing (DLP)* is similar but uses a digital light projector to cure the resin, allowing for faster curing times and higher efficiency in some applications.

Material Jetting deposits droplets of material onto a build platform and cures them to form objects. *Inkjet Printing* is a technique within this category, known for its ability to create high-resolution and multi-material objects.

Binder Jetting involves the deposition of a liquid binding agent onto a powder bed. The binder selectively joins the powder particles to form each layer of the object. This technique can be used with a variety of materials, including metals, ceramics, and sand.

Bioprinting is a specialized type of 3D printing used to create structures that mimic the natural tissues found in the body. This technique typically involves the use of bio-inks made from living cells and biocompatible materials to print complex tissue structures for medical applications, such as tissue engineering and regenerative medicine.

Each 3D printing technology has its unique advantages and limitations, making them suitable for different applications across various industries. Among these, FDM and SLA/DLP are the most widespread and popular due to their cheapness and accessibility.

With the development and reduction in cost of 3D printing technology, the production of artificial reservoir rock structures has received a new boost. The widespread availability and affordability of 3D printers have democratized the production of complex structures, allowing researchers and institutions to use them in a variety of scientific projects.

A plethora of scientific studies have delved into the realm of 3D printing of reservoir pore structures, exploring various aspects such as replicating natural formations, understanding fluid dynamics, and developing synthetic cores for experimental studies. This synthesis of research highlights the technological advancements and applications of 3D printing in geoscience.

3D printing has significantly advanced the study of pore structures in composite materials and reservoir rocks by allowing researchers to replicate and examine complex geological features with precision. Ishutov et al. [10] were early adopters of this technology for replicating sandstone porosity models, which demonstrated the potential of 3D printing in visualizing pore connectivity and geometry at the microscale. Their work established a foundation for further studies into the application of additive manufacturing in petrophysical research.

Subsequently, Ishutov et al. [11] replicated carbonate reservoir pores at their original size, achieving a detailed representation of pore structures that were accurate to 20 mm in scale. This development facilitated a deeper understanding of the influence of pore geometry on reservoir properties and fluid flow dynamics. Ma et al. [12] have also contributed to this field by exploring the systematic use of 3D-printed rocks for petrophysical studies, emphasizing the technology's potential to replicate intricate pore networks for detailed analysis. Mukhametrakhimov et al. [13] expanded this research by employing X-ray computed tomography to

analyze the structure of 3D-printed concrete, demonstrating the precision with which additive manufacturing can capture fine-scale details of composites. Their work contributes to our understanding of the mechanical and structural properties of construction materials.

Studies have also highlighted the use of 3D printing to enhance experimental methodologies in petrophysics and rock mechanics. Kong et al. [14] provided a comprehensive review of the applications of 3D printing in these fields, discussing the technology's ability to create accurate models for testing and analysis. Almetwally and Jabbari [8,15] conducted experiments on 3D-printed rock samples, examining their mechanical properties and establishing methods to replicate natural geological materials in lab settings. These studies have underscored the potential for 3D printing to innovate experimental approaches, allowing researchers to explore various scenarios and optimize recovery techniques in reservoir engineering.

In terms of fluid dynamics, Song et al. [16] investigated the flow properties in 3D-printed natural sandstone at the pore scale, providing insights into single and multiphase flow behaviors. Similarly, Wang et al. [17] designed rock-based microfluidics using 3D printing to validate pore-scale flow experiments, demonstrating the technology's ability to replicate intricate pore structures for detailed fluid dynamics studies. Goral and Deo [18] further advanced this area by fabricating synthetic nanoporous geomaterials, bridging nanoscale imaging with 3D printing to explore digital rock technologies and enhance the accuracy of petrophysical analyses.

The adaptation of 3D printing in experimental setups has also led to significant advancements in synthetic core plug development. Cruz-Maya et al. [6,19] explored the use of synthetic core plugs as alternatives to natural ones for core flooding tests, enabling researchers to conduct controlled experiments to assess reservoir scenarios. These studies demonstrated that synthetic cores can provide valuable insights into fluid flow and reservoir behavior under various conditions. Stoporev et al. [20] also leveraged 3D-printed polymeric cores to study enhanced methane hydrate growth, illustrating how 3D printing can simulate complex chemical interactions within porous media. This work complements other studies focused on fluid dynamics within printed structures, highlighting the potential of 3D printing to innovate experimental methodologies in reservoir engineering and geosciences.

Additionally, the use of 3D printing for microfluidic applications has been explored by Li et al. [21], who integrated micro-3D printing with mineral coatings to enhance device capabilities for studying fluid behaviors in tight reservoirs. This approach underscores the potential for 3D printing to innovate experimental methodologies in rock mechanics and petrophysics. Furthermore, Wang et al. [22] analyzed the effect of porosity on the mechanical properties of 3D-printed polymers using X-ray computed tomography, demonstrating how this technology can be used to optimize material properties and structural designs.

The ability to precisely reproduce the intricate pore network of authentic samples offers a promising solution to the challenge of varying pore structures among core samples. By employing advanced 3D printing techniques, scientists can generate replicated samples that mimic the exact pore space characteristics of the original cores. These replicated samples can serve as valuable tools for mitigating the diversity influence of pore structures in different experiments, ensuring a more uniform testing ground.

Furthermore, these 3D-printed clones hold potential beyond standardizing pore structures. They could be utilized as reference materials, acting as benchmarks for the calibration and cross-verification of measurement instruments. By comparing measurements obtained from identical 3D-printed replicas, researchers can assess the accuracy and reliability of their analytical tools. This approach not only enhances the precision of measurements but also instills confidence in the experimental results, addressing the uncertainties stemming from the inherent variations in natural core samples.

Additionally, the application of 3D-printed standard clones can extend to educational and training purposes. These replicas can serve as invaluable teaching aids, providing students with hands-on experience in core analysis without the constraints of limited and irreplaceable natural samples. Through interactive experiments with these cloned specimens, future scien-

tists and engineers can hone their skills, deepen their understanding, and explore innovative techniques, fostering the growth of expertise in the field.

With the advancement of 3D printing technology, the production of artificial core samples has become significantly more economically viable than traditional core sampling methods. The widespread availability and affordability of 3D printers have democratized the production of complex structures, enabling researchers and institutions use it in different scientific projects.

The objective of this study is to explore the potential of 3D cloning for replicating the reservoir structure of standard core plugs. It includes μCT scanning, digital processing, and 3D printing using cost-effective methods like FDM and DLP. By performing repeated μCT scans of the printed 3D clones and comparing their structural and filtration characteristics with those of the original core plugs, the study assesses the effectiveness and accuracy of the cloning process. The study focuses on detailing effective methodologies for creating 3D-printed replicas, highlight process nuances, and critically analyze technological constraints to identify areas for improvement and innovation. This research seeks to deepen understanding of the 3D structure cloning process in core plug scale and support future advancements in the field.

2. Materials and methods

2.1. μCT of core plug

To assess the feasibility of replicating the effective pore structure of a standard sample, a carbonate core plug with a diameter of 30 mm and a height of 30 mm was selected from the Vereyian deposits of one of the oil fields in the Republic of Tatarstan. The sample's oolitic structure features relatively large filtration pores, which is important due to the resolution limitations of modern FDM and SLA/DLP printers.

Using μCT, a 3D image of the core plug was obtained. Imaging was performed using the General Electric Phoenix V|tome|X S 240 [23], a micro- and nanofocus X-ray system. The system operated with a nanofocus tube at 130 kV and 140 mA, capturing a total of 1200 projections with 3 projections averaged, and 200 ms exposure time per projection. The imaging resolution of the sample was 18 μm. Voxel model reconstruction was carried out using Phoenix Datos|x reconstruction software [24]. The resulting volumetric image is a voxel array saved in vol format with a metadata file in vgi format. Subsequent digital processing and calculations of the volumetric model characteristics were performed using Avizo software [25].

At the first stage, a digital model of the sample surface was obtained, followed by segmentation of the effective porosity structure. This segmentation was carried out by connecting the selected voxels from one end of the cylindrical sample to the other along the z-axis, allowing for the identification of effective porosity. Then, the distribution of the equivalent pore diameters for this pore structure was determined. The pore distribution analysis by equivalent diameters involved several steps. First, pore chambers within the volume of connected porosity were separated by the throats [26]. Next, the equivalent diameters of these pores were measured as the diameter of a sphere that has the same volume as the pore (Vp):

$$D_{eq} = \sqrt[3]{\frac{6 \times V_p}{\pi}} \tag{1}$$

These measured diameters were then grouped into distinct diameter intervals. A distribution diagram was subsequently plotted to show the equivalent pore diameters across these intervals, illustrating their percentage share (%) of the total connected porosity volume.

The maximum printing resolution of most FDM and SLA/DLP printers (50-100 μm) is significantly lower than the resolution of the obtained digital model (18 μm). Pore size analysis showed that the effective porosity structure of the sample contains pores smaller than the printing resolution, which would lead to breaks in the narrowed areas of the effective porosity pore channels during printing, resulting in a lack of permeability. Additionally, the real pore

structure surface obtained from μCT has an extremely complex shape. Therefore, a special method of digital processing were proposed to simplify the pore structure shape and maintain the sample's filtration capacity after 3D printing.

2.2. Digital processing of core plug pore structure for 3D printing

Although the carbonate core plug structure contains many large pores, the effective porosity structure is characterized by numerous channel constrictions and complex morphology, which poses challenges for 3D printing. The first issue leads to the filament filling narrow channels during 3D printing due to the resolution limitations of the printers used, resulting in breaks in the filtration channels within the pore structure. The second issue causes excessive meshing time (up to several days), often ending in errors and difficulties in slicing the model. Therefore, we developed a method to process the 3D structure of effective porosity, which slightly enlarges pore sizes and simplifies their morphology. However, it allows for reliable printing of the core plug model with a permeable structure using popular FDM printers with standard 0.4-0.2 mm nozzles and SLA/DLP printers. This approach to creating a unified 3D printing model aligns well with the research goals and facilitates comparing different 3D printing techniques based on the evaluation of the pore structure parameters of printed clones.

The digital processing method was implemented using Avizo software and involved expanding the boundaries of the effective pore space (the “Dilation” operation) by 2 voxels in 3D space (or by 4 voxels in pore diameter) and smoothing the surface of the effective pore structure. The expansion parameters included a connectivity value set to 6, where voxels with a shared face were considered connected. Subsequently, the resulting volume was smoothed using the “Binary Smoothing” operation, with smoothing parameters including a voxel size of 2 along the X, Y, and Z axes. Then, a procedure was carried out to remove excessive small, unconnected pores using the “Erosion” operation with parameters set to a ball type and size of 1 voxel. Since the erosion operation significantly reduces the volume of effective pores, the “Dilation” operation was reapplied with the same parameters.

After processing the volume of effective porosity, its volume was subtracted from the three-dimensional volume of the sample model, which was solid (without pores. The resulting voxel model of the sample matrix was converted into surface models (meshes) and saved in the stl format.

2.3. FDM and DLP printing methodology

The generated sample matrix model was used for 3D printing using FDM technology with 0.4 mm and 0.2 mm nozzles and DLP technology. In total, three core plug samples were printed.

FDM printing was performed using the Raise3D Pro 2 [27], a 3D printer designed for high-precision printing. Slicing was performed using Ideamaker 5.0.6 software [28]. ABS plastic with a diameter of 1.75 mm was used as the printing material. For Sample 1, the printing parameters were: nozzle diameter of 0.4 mm, layer height of 0.2 mm, 100% infill, printing speed of 60 mm/sec, nozzle temperature of 250 °C, and bed temperature of 100 °C. The printing parameters for Sample 2 included a nozzle diameter of 0.2 mm, a layer height of 0.1 mm, 100% infill, a printing speed of 60 mm/sec, a nozzle temperature of 250 °C, and a bed temperature of 100 °C.

DLP printing was performed using an Anycubic Photon Mono X photopolymer printer with an 8.9’ LCD 4K display and a printing resolution of 50 μm [29]. Slicing was conducted using the Anycubic Photon Workshop application [30]. Anycubic Photon photopolymer resin was used, which has the following properties: hardness of 79D on the Shore scale, viscosity (at 25 °C) of 552 mPa*s, liquid density of 1.1 g/cm^3, solid density of 1.184 g/cm^3, shrinkage of 7.1%, tensile strength of 23.4 MPa, and elongation at break of 14.2%. After printing, the sample was cleaned of excess resin using an alcohol washing procedure with a Hassler-type core

holder from the Wille Geotechnik filtration unit [31]. After printing, the model underwent curing under a UV lamp.

2.4. Evaluation of the characteristics of printed plugs

To evaluate the pore structure of the printed samples, μCT was used again. The scanning parameters for evaluating the printed plugs were similar to those used for the original sample, except that the tube voltage was reduced to 130 kV. The microtomography resolution for all plastic plugs was 18.8 μm. In the resulting digital models of the printed plugs, segmentation of the effective porosity was performed, and the porosity coefficient (for pores larger than 18.8 μm), pore surface area, and pore volume were determined. The specific surface area was calculated based on the ratio of these measurements. Additionally, for each printed sample, the pore size distribution was constructed using equivalent diameter based on the methodology described in section 2.1.

Furthermore, measurements of the filtration properties and pore volume were conducted for both printed and original samples. Open porosity was measured using nitrogen with a PIK-PP gas porosimeter-permeameter [32]. Water permeability was determined using a Wille Geotechnik filtration setup. The method involves placing the sample in a core holder with a sleeve that ensures sealing at a confining pressure of 1.5 MPa. Filtration of deionized water was carried out at a constant flow rate, with monitoring of steady flow established by the stability of the pressure drop. The flow is considered stable when three consecutive measurements differ by no more than 2%.

3. Results and discussion

3.1. 3D-clones analysis

As a result of the study, three clones of standard core plug (Fig. 2A) were successfully produced from its digital model after processing the pore space structure (Fig. 2B) the using 3D printing techniques. Two samples were fabricated using the FDM method, utilizing nozzle sizes of 0.4 mm (Fig. 2C) and 0.2 mm (Fig. 2D), respectively, and one sample was produced using DLP printing (Fig. 2E). The surfaces of the original core plug and the printed clones exhibit similar structural characteristics. Large pores and dense regions are distributed in a comparable manner across both the original sample and the 3D-printed replicas.

On the surface of the FDM 0.4 mm sample, larger pores and a rougher texture are noted, with pronounced striations formed by the printing lines in the denser regions of the sample. The pores on the surface of the FDM 0.2 mm sample are noticeably smaller, and the surface is smoother. The DLP sample exhibits the smallest pores among all samples; however, its surface also displays numerous micro-cracks that interconnect various pore clusters.

The visualization of the structural differences on orthoslices among the original carbonate core plug, processed digital model and 3D-printed clones presented in Fig. 3. The reference sample (A) displays a uniformly distributed tiny pore structure, highlighting the challenge faced by the 3D printing techniques. The digital model (B), developed based on the methodology described in part 2.2 and utilized for the 3D printing of all subsequent samples, shows slightly expanded pores with a smoothed pore surface structure. When examining the FDM-printed clones, significant differences in pore structure emerge: the clone printed with a 0.4 mm nozzle (C) exhibits coarser texture and larger voids, reflecting the limitations in resolution inherent to this printing method. In contrast, the 0.2 mm nozzle FDM clone (D) demonstrates finer pore replication, achieving a smoother surface finish, though some loss of detail compared to the original is evident. The DLP-printed clone (E) provides the most intricate replication of pore structures, capturing finer details and closely resembling the digital model. However, it also reveals a network of micro-cracks that could potentially influence pore connectivity.

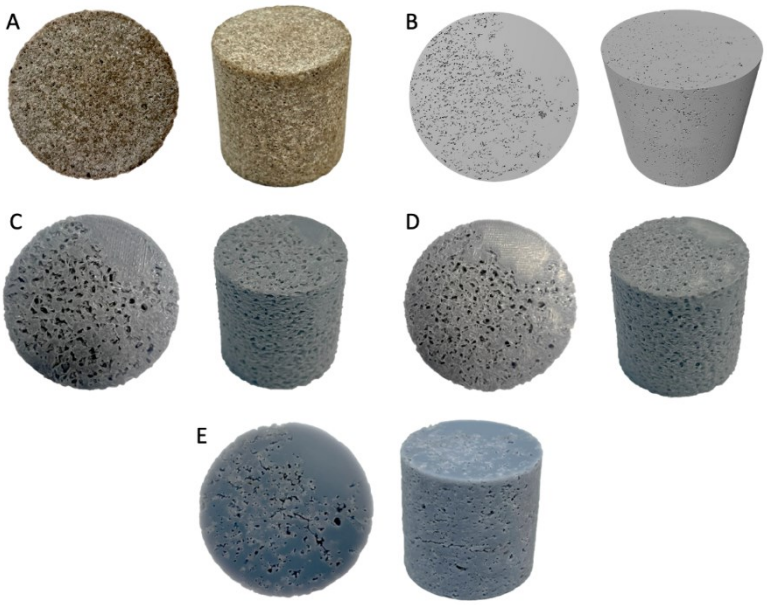

Fig. 2. Results of standard core plug 3D-cloning: A – reference carbonate core plug, B – digital model after processing the pore space structure, C – FDM-printed clone with nozzle of 0.4 mm, D – FDM-printed clone with nozzle of 0.2 mm, E – DLP-printed clone

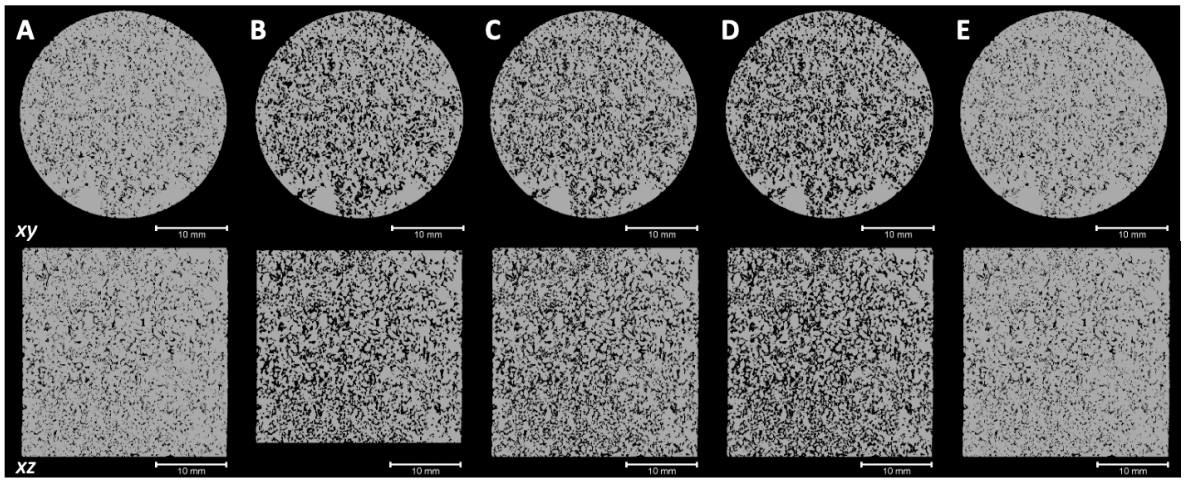

Fig. 3. Orthoslices of the samples in the xy (top row) and xz (bottom row) projections: A – reference carbonate core plug, B – digital model after processing the pore space structure used for 3D printing all clones, C – FDM-printed clone with a nozzle of 0.4 mm, D – FDM-printed clone with a nozzle of 0.2 mm, E – DLP-printed clone.

Zoomed pore structures reveal intricate pore channels nestled between rounded mineral matrix elements in the original core sample (Fig. 4A). In the digitally processed model, the thin pore channels are significantly expanded, and the overall pore structure is smoothed out (Fig. 4B). The FDM-printed clone with a 0.4 mm nozzle shows extensive voids within and a pore morphology that is distinctly different from the original model, with the structure being difficult to correlate across both the xy and xz planes (Fig. 4C). Additionally, there is noticeable flattening of the matrix structure in the vertical (Z) direction, forming horizontal patterns likely due to layer thickness reduction during printing to 0.2 mm. In the FDM-printed clone with a 0.2 mm nozzle, the pore structure is closer to the original model, although it is still significantly expanded, sometimes merging fine pore channels into larger single voids (Fig. 4D). The DLP-printed clone most accurately replicates the original morphology of the digital model, both in horizontal and vertical planes (Fig. 4E). However, even in this model, the pore

structure is slightly expanded compared to the original digital model, albeit less than in the other clones.

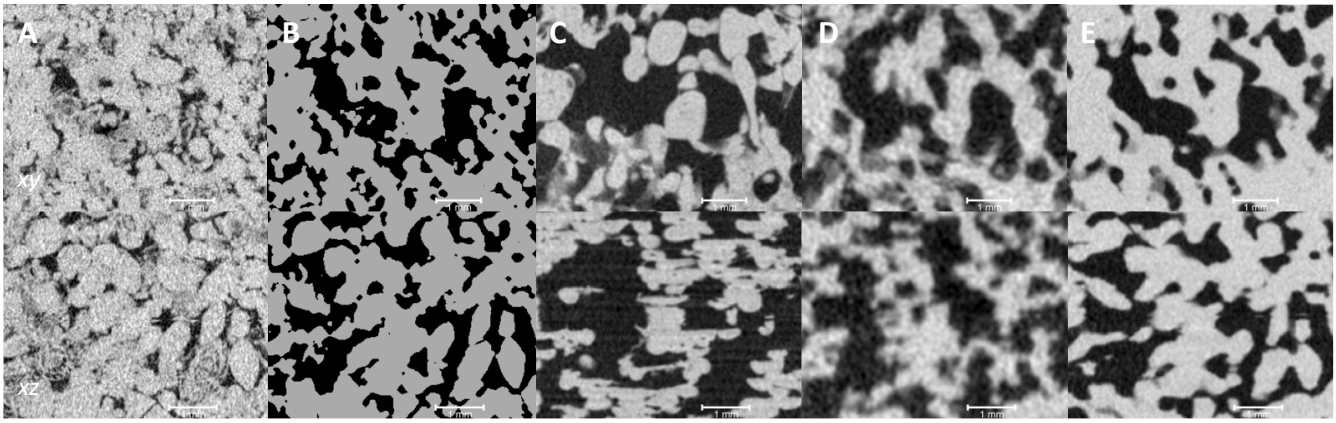

Fig. 4. Zoomed pore structure orthoslices of the samples in the xy (top row) and xz (bottom row): A – reference carbonate core plug, B – digital model after processing the pore space structure used for 3D printing all clones, C – FDM-printed clone with a nozzle of 0.4 mm, D – FDM-printed clone with a nozzle of 0.2 mm, E – DLP-printed clone.

The analysis of the μCT and experimental data reveals significant differences between the original carbonate core plug, its digital model, and the 3D-printed clones. The original sample (A) demonstrates a total porosity of 10.22% and an effective porosity of 9.5%, with a high specific surface area of 43.67 mm^{-1}. Experimental measurements indicate an open porosity of 14.25% and permeability values of 617.89 mD for gas and 308.27 mD for water, which is indicative of a moderately permeable rock with interconnected pore spaces.

The digital model (B), derived from image processing and used as a reference for 3D printing, shows a slight increase in both total and effective porosity to 11.59%. However, the specific surface area decreases to 38.73 mm^{-1}, suggesting some smoothing of the pore structure during digital processing. This model serves as a benchmark for comparing the 3D-printed clones, though it does not have associated experimental permeability data.

Among the 3D-printed clones, the FDM-printed samples with 0.4 mm (C) and 0.2 mm nozzles (D) demonstrate significantly higher total and effective porosities, both around 36%, compared to the original sample. The open porosities are closely aligned with the μCT-derived porosities, confirming that under the applied confining pressure, the plastic pore spaces and cracks slightly compress, leading to porosity values close to those obtained via μCT-imaging. These elevated porosity values are accompanied by lower specific surface areas (9.75 mm^{-1} and 8.82 mm^{-1} respectively), suggesting that the FDM printing process introduces more extensive but less intricate pore structures. This structural alteration results in much higher gas and water permeability values, with gas permeability exceeding 15,000 mD and water permeability ranging from 1,700 to 1,750 mD, which are significantly higher than those of the original sample.

The DLP-printed clone (E) presents a more moderate increase in total (16.52%) and effective porosity (16.14%) compared to the original. The specific surface area of 12.01 mm^{-1} is higher than that of the FDM clones, indicating better retention of fine pore structures. The open porosity of 14.88% is slightly higher than the original, suggesting that the DLP method produces a more accurate replication of the pore structure under confining pressure. Despite the more detailed pore network, the gas permeability is markedly lower at 1,582.1 mD, and the water permeability is also lower at 1,265.23 mD, reflecting a more restricted fluid flow through the finer pore channels of the DLP-printed clone.

Table 1. A comparison between the original carbonate core plug and its 3D-printed clones based on µCT data and experimental measurements

Sample	µCT data			Experimental data		
	Total porosity, %	Effective porosity, %	Specific surface, mm^{-1}	Open porosity, %	Gas permeability, mD	Water permeability, mD
Original (A)	10.22	9.5	43.67	14.25	617.89	308.27
Digital model (B)	11.59	11.59	38.73	-	-	-
FDM 0.4 mm (C)	36.61	36.3	9.75	36.53	15860.7	1746.76
FDM 0.2 mm (D)	36.44	36.09	8.82	36.36	17014.4	1711.61
DLP (E)	16.52	16.14	12.01	14.88	1582.1	1265.23

The pore size distribution analysis presented in the graphs (Fig. 5) reveals significant differences between the original carbonate core plug (A), the digital model (B), and the 3D-printed clones (C, D, E). The original sample (A) exhibits a narrow pore size distribution, with the majority of pores concentrated around smaller diameters, indicating a tight pore network. The digital model (B), although based on the original structure, shows a slight shift towards larger pores due to the smoothing and processing involved in model preparation. In contrast, the FDM-printed clones (C, D) display much broader pore size distributions with peaks at larger diameters, particularly in the clone printed with a 0.4 mm nozzle (C). This shift indicates the presence of larger interlayer spaces between the printed lines, which inflate the effective porosity and alter the pore network morphology. The DLP-printed clone (E) achieves a more precise replication of the original pore size distribution, with most pores concentrated around smaller diameters, closer to the original core plug. However, some slight expansion of the pore sizes is still observable, likely due to the inherent limitations of the DLP printing process.

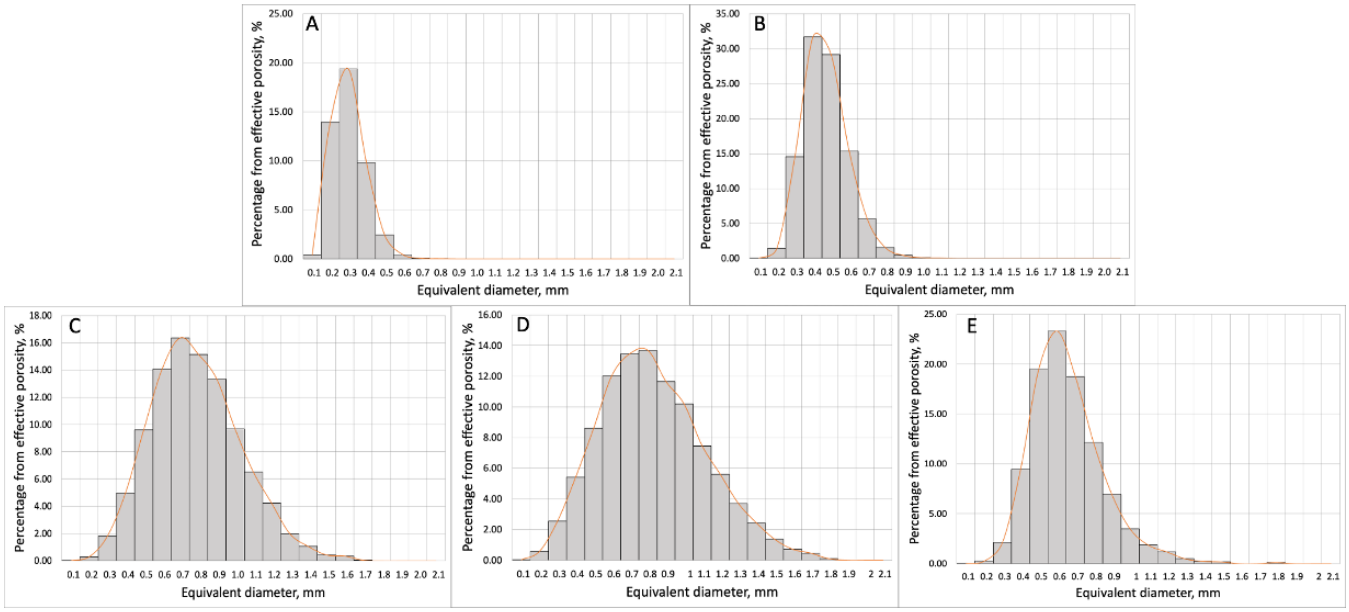

Fig. 5. Distribution of equivalent diameters versus effective porosity (in %) for the original carbonate core plug (A), digital model (B), and 3D-printed clones (C: FDM 0.4 mm, D: FDM 0.2 mm, E: DLP

Various structural anomalies have been observed in the 3D-printed core samples produced by FDM and DLP techniques (Fig. 6). In the FDM-printed clone with a 0.4 mm nozzle (Fig. 6A), clear interlayer gaps are visible, which contribute significantly to the artificially elevated porosity and permeability values. These gaps distort the true pore structure of the original carbonate rock, creating voids that are not representative of natural pores. Similarly, in the FDM-printed clone with a 0.2 mm nozzle (Fig. 6B), although the interlayer gaps are some-

what finer, they still result in exaggerated porosity and permeability readings. Further examination of the 0.2mm FDM clone (Figure 6C) reveals the presence of a fiber component in the pore space, which, together with the interlayer gaps, are unintentional artifacts of the printing process. These fibers further alter the flow paths within the pore network, potentially obstructing or redirecting fluid movement, thereby complicating the interpretation of permeability measurements. Finally, the DLP-printed clone (Fig. 6D) shows the presence of residual resin within the pores, which can occlude the pore throats and reduce effective porosity and permeability. This residual material might also suggest incomplete curing during the DLP printing process, which could impact the mechanical properties and the accuracy of the pore structure replication.

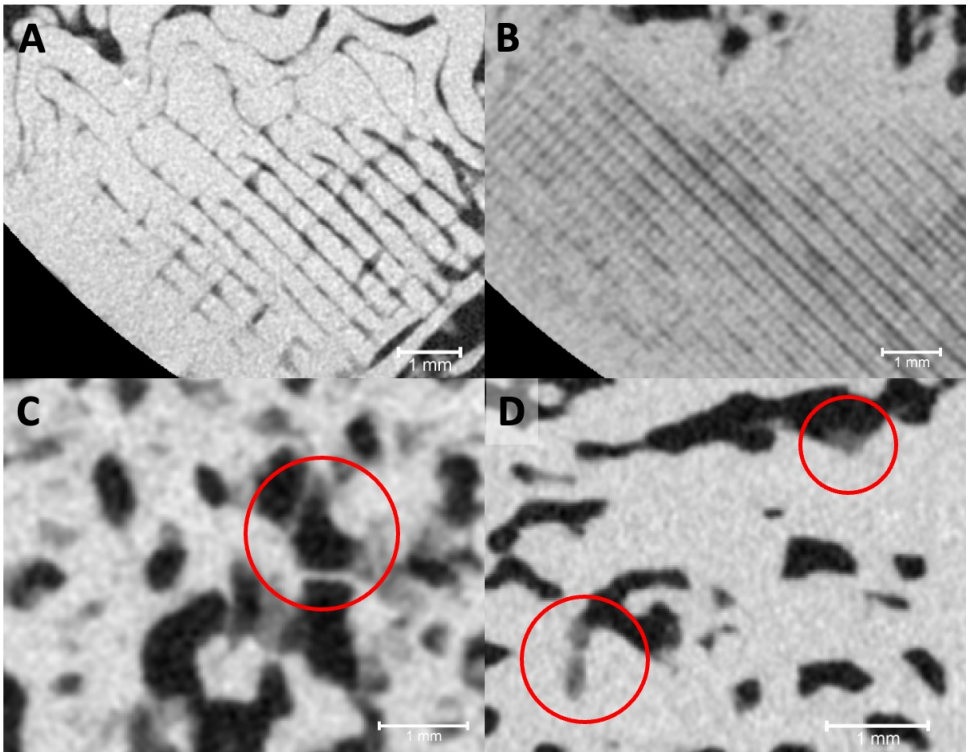

Fig. 6. Structural artifacts observed in 3D-printed core samples: A - FDM (0.4 mm) showing interlayer gaps that lead to inflated porosity and permeability values; B - FDM (0.2 mm) with smaller interlayer gaps still affecting measured properties; C - FDM (0.2 mm) highlighting extraneous fibers within pore spaces; D - DLP revealing residual resin obstructing pores

3.2. Printing stability check

To assess the stability and repeatability of the pore structure in 3D-printed core clones, we printed three samples using the FDM method with a 0.2 mm nozzle and three samples using the DLP method. For the FDM prints, the same G-code file was used, ensuring that each print was based on an identical STL model and consistent printing parameters. For the DLP prints, we utilized the equivalent *photon format files specific to the Anycubic Photon Mono X printer, which were generated from the same STL model but with parameters optimized for DLP printing.

Following the 3D printing process, each clone was subjected to repeat µCT-scanning to analyze the internal structure of the pore space. Additionally, wherever possible, we measured the filtration and reservoir properties of these clones, using methods analogous to those presented in section 3.1. This approach ensures that any variations observed in the printed samples can be attributed to the inherent stability and precision of each 3D printing technique, rather than differences in the input files or settings. Consequently, this method allows for a rigorous comparison of the reliability of FDM and DLP printing in consistently replicating the desired pore structures across multiple prints.

The results of 3D printing three clones using the FDM method with a 0.2 mm nozzle are presented in Fig. 7. It is observed that the pore structures on the surface of all three 3D clones exhibit similar pore distribution and sizes. When examining the pore structures in the μCT slices of the 3D-printed clones (Fig. 8), it becomes evident that while most of the larger pores are consistently present across all samples, a significant number of pores appear in some clones but are entirely absent in others. Upon closer examination of the μCT slices for the three FDM 0.2 mm nozzle clones (Fig. 9), it is apparent that while the general morphology of larger pores is consistent across all samples, there are notable discrepancies in the presence of smaller pore elements. These smaller features are sometimes entirely missing in one or more of the clones, even though they are present in others. This observation suggests that despite the general similarity in pore distribution and size on the surface, there are notable inconsistencies in the replication of the pore space across different clones. These inconsistencies could be attributed to slight variations in the printing process, such as minor fluctuations in layer adhesion or material deposition, which can lead to the presence or absence of certain pore features in the final printed structures. This variability highlights the challenges in achieving perfect reproducibility of complex pore structures using the FDM method, even when the same G-code is used.

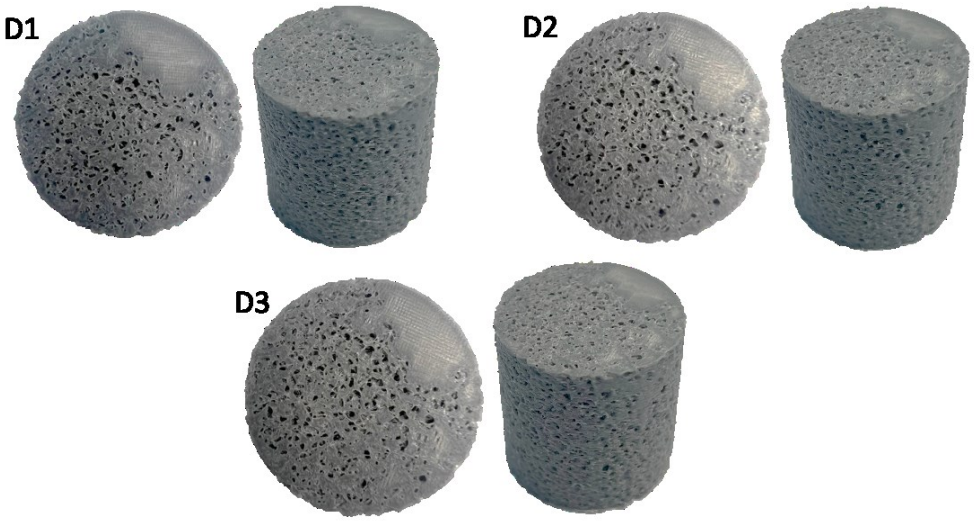

Fig. 7. Three clones printed using the FDM method with a 0.2 mm nozzle from the same G-code file. Sample D1 corresponds to the sample labeled D in Fig. 2.

The analysis of μCT images for the 3D-printed clones using FDM with a 0.2 mm nozzle (table 2) reveals significant variations in total and effective porosity across the different samples, with values ranging from 28.09% to 36.44% for total porosity and 27.06% to 36.09% for effective porosity. These differences highlight the variability inherent in the 3D printing process, particularly in replicating the fine details of pore structures in each clone. Such variations can be attributed to the challenges in consistently reproducing small pore features across multiple prints, which impacts the overall porosity measurements. Despite these variations in porosity, the specific surface area, as determined by μCT data, remains relatively consistent among the three clones, ranging from 8.46 mm^{-1} to 8.82 mm^{-1}. This consistency suggests that the main pore structure, including the overall morphology and volume, is largely preserved across the different 3D-printed samples. The close similarity in specific surface area indicates that the bulk of the pore network is effectively replicated, even if minor details vary between prints.

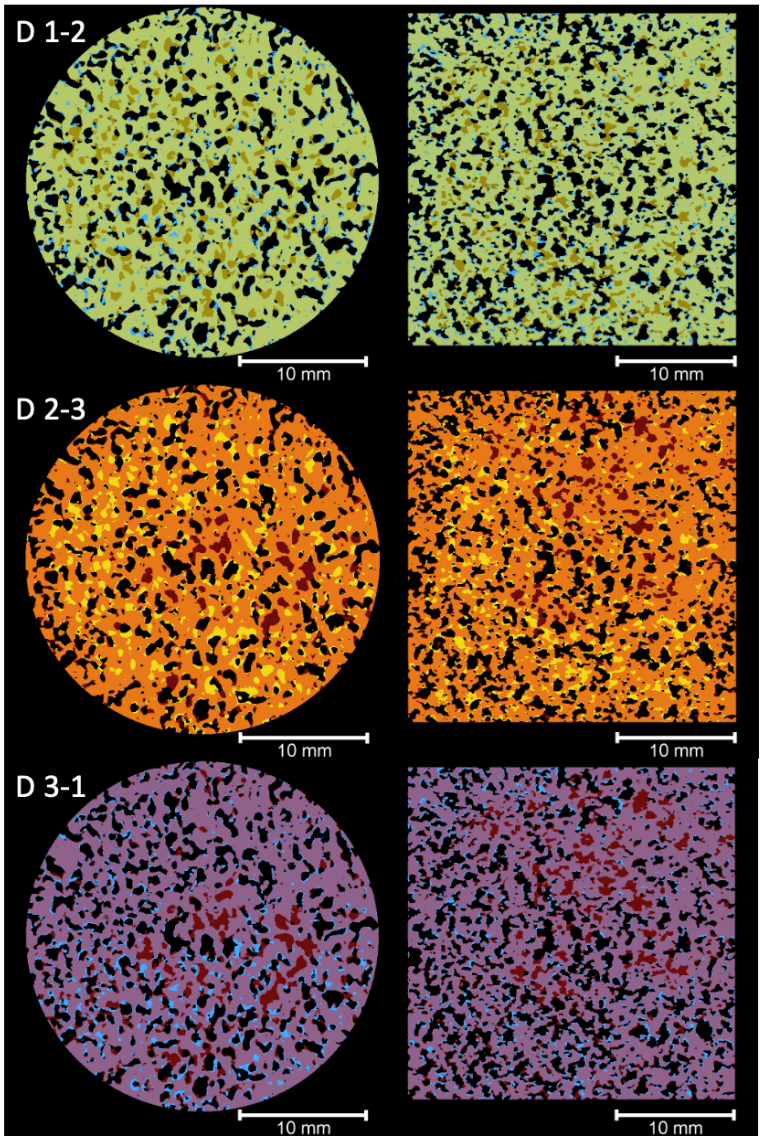

Fig. 8. Overlapping slices in XY (left) and XZ (right) projections for three FDM-printed clones using the 0.2 mm nozzle: D1 - blue, D2 - yellow, D3 - red. Areas where colors mix indicate regions successfully printed in both 3D clones, while regions where one color remains indicate a lack of print in that area in the other clone.

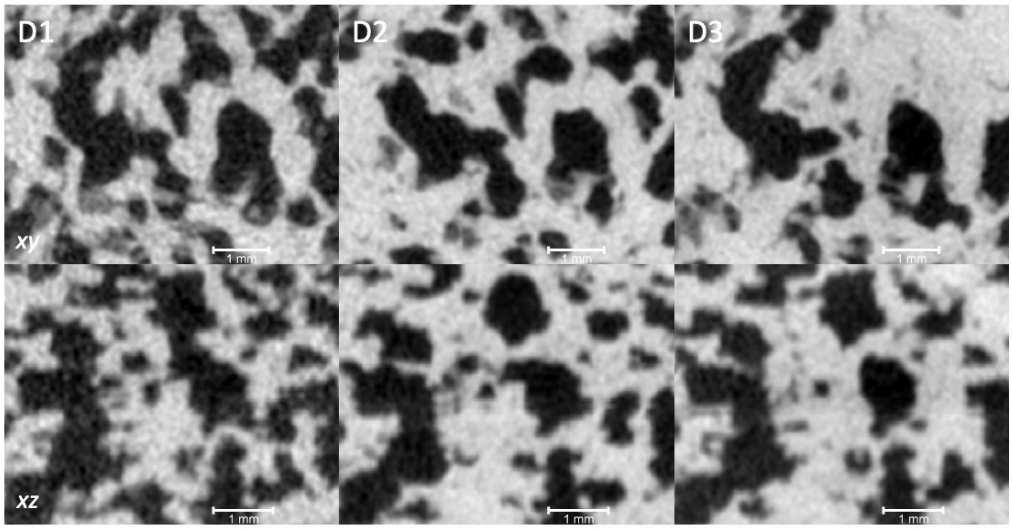

Fig. 9. Zoomed pore structure orthoslices of the samples in the xy (top row) and xz (bottom row) for three FDM-printed clones using the 0.2 mm nozzle

The experimentally measured open porosity also shows close agreement across the clones, with values clustering around 36%. Interestingly, in some cases, the open porosity measured experimentally is slightly higher than the total porosity determined by μCT. This discrepancy could be due to the presence of interlayer porosity, which is not fully captured by the resolution of the μCT imaging. The high similarity in open porosity values confirms the replicability of the porosity characteristics across the clones, while the slight excess suggests that sub-resolution pores, possibly formed between printed layers, contribute to the overall porosity but are not detected by μCT.

Table 2. A comparison among three FDM clones printed with the 0.2 mm nozzle based on μCT data and experimental measurements

Sample	μCT data			Experimental data		
	Total porosity, %	Effective porosity, %	Specific surface, mm^{-1}	Open porosity, %	Gas permeability, mD	Water permeability, mD
FDM 0.2 mm (D1)	36.44	36.09	8.82	36.36	17014.4	1711.61
FDM 0.2 mm (D2)	28.09	27.06	8.67	36.67	20584.5	1878.1
FDM 0.2 mm (D3)	33.24	32.67	8.46	36.79	18540.2	1854.2

Finally, the differences in gas and water permeability across the samples underscore the significant impact that small pore features can have on the flow properties of the materials. The variation in permeability values indicates that even minor differences in pore geometry and connectivity can lead to substantial changes in the flow behavior of the printed materials. This highlights the importance of accurately reproducing pore structures to achieve consistent filtration properties in 3D-printed materials.

The pore size distribution analysis for the 3D-printed clones using FDM with a 0.2 mm nozzle (Fig. 10) confirms that the primary pore structure is well preserved across the samples. In all cases, the distribution diagrams exhibit a similar pattern, with a prominent peak in the 0.6-0.8 mm range. This consistency indicates that the main framework of the pore network remains intact, ensuring that the overall porosity characteristics are effectively replicated in the printed clones. Noticeable variations in the distribution are only observed for pores with equivalent diameters smaller than 0.6 mm. These differences suggest that while the larger pore structures are faithfully reproduced, the finer details of the smaller pores are more susceptible to discrepancies during the 3D printing process.

The results of the DLP printing of three clones are shown in Fig. 11. After printing, each sample was subjected to an isopropyl alcohol wash to remove any uncured photopolymer resin, followed by curing under UV light. During this curing process, cracks formed in all samples. Notably, while the cracks in sample E1 are relatively small, samples E2 and E3 exhibited larger cracks that split the samples into multiple segments.

The occurrence of these cracks during DLP printing is primarily due to the internal stresses that develop as the resin cures and solidifies. DLP printing involves the layer-by-layer photopolymerization of resin, and each layer undergoes shrinkage as it hardens. The accumulated stress from this shrinkage, particularly in areas with significant differences in thickness or unsupported regions, can lead to cracking. Moreover, the presence of pores in the samples likely exacerbated the stress concentration, leading to more severe cracking in E2 and E3.

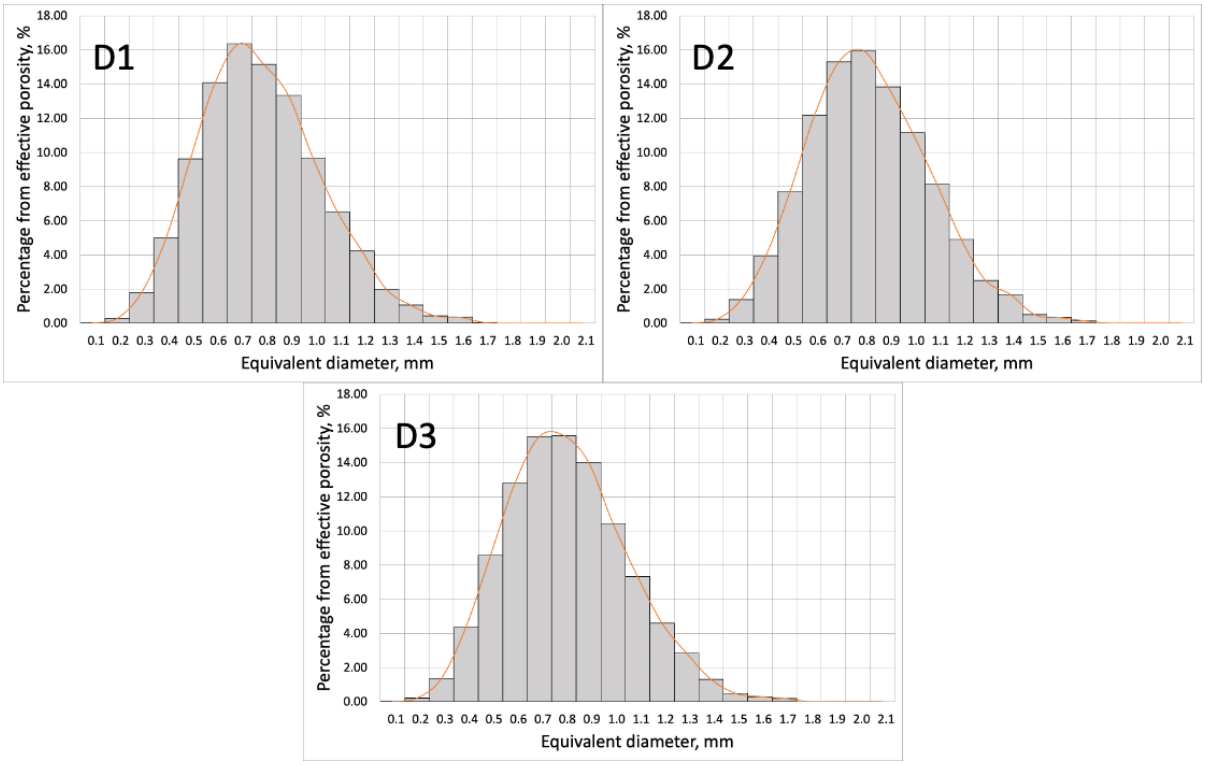

Fig. 10. Distribution of equivalent diameters versus effective porosity (in %) for three FDM-printed clones using the 0.2 mm nozzle

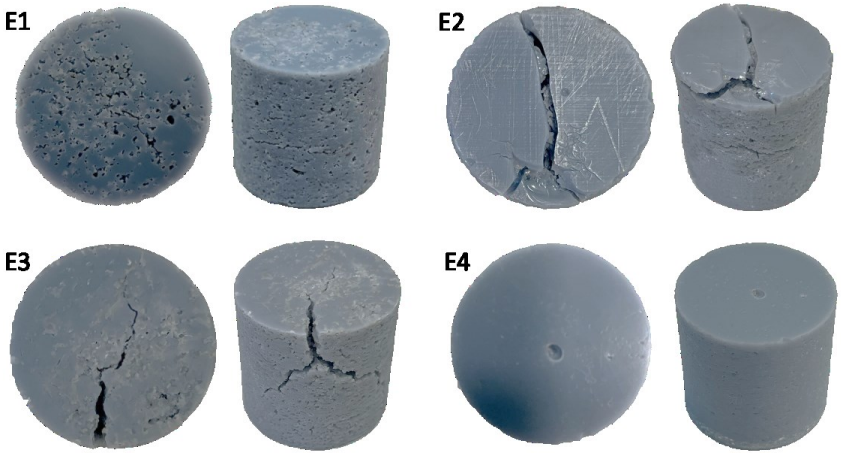

Fig. 11. Three clones (E1-E3) printed using the DLP method from the same file (photon format). Sample E1 corresponds to the sample labeled E in Fig. 2. Sample E4 is a solid specimen that lacks internal pores, which contributes to its resistance to crack formation during the solidification process.

Interestingly, when a solid sample without internal pore structures was printed (sample E4), no cracking was observed (Fig. 11E4). This suggests that the absence of internal pores minimizes stress concentration during curing, thereby preventing the formation of cracks. The reduced crack formation in E1 may be more closely related to the specifics of the curing process, particularly the duration and uniformity of UV exposure. Variations in the curing process, such as the duration or intensity of UV light, could result in differing levels of internal stress within the samples, influencing the extent and severity of crack formation. Understanding and optimizing the curing process is crucial for minimizing defects like cracks in DLP-printed structures. Therefore, a more in-depth study is necessary to fully comprehend the impact of curing conditions on the structural integrity of 3D-printed samples.

Despite the formation of cracks in the samples, it was still possible to select intact areas near the pores for analysis using μCT imaging (Fig. 12). The analysis revealed that while the morphology of basic pores is well-preserved across all samples, smaller pore elements or even entire small pores are sometimes entirely absent. This suggests that although DLP printing offers higher accuracy and fidelity in maintaining the morphology of large pores, it encounters similar challenges to FDM printing when it comes to accurately replicating fine pore structures. This limitation underscores the difficulties in capturing small-scale details during the 3D printing process, regardless of the printing method used.

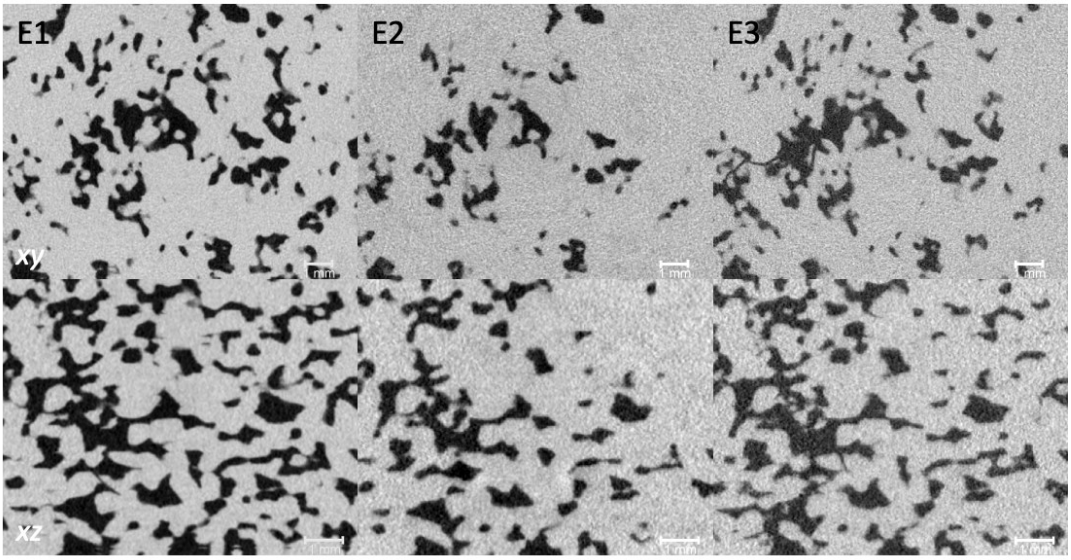

Fig. 12. Zoomed pore structure orthoslices of the samples in the xy (top row) and xz (bottom row) for three DLP-printed clones

4. Conclusion

In this study, we primarily investigated the feasibility of using the most accessible 3D printing methods, FDM (Fused Deposition Modeling) and DLP (Digital Light Processing), for 3D cloning core plugs. Our focus was on assessing the stability and reproducibility of the pore structures in the 3D-printed core clones. We systematically analyzed the printed samples using μCT scanning and performed experimental measurements of porosity and permeability to evaluate the fidelity of pore replication across multiple prints.

We came to the following key points in the course of our work:

– Both FDM and DLP printing methods exhibit a resolution limit below 50 μm, which is lower than the resolution of μCT models (18 μm) and far below the scale of transport pores in reservoir rocks. This resolution gap highlights the inherent challenges in accurately reproducing the fine-scale features of reservoir pore structures. Additionally, the 3D pore structure derived from μCT data possesses highly complex morphology, necessitating significant optimization in the form of surface expansion and smoothing to make it suitable for 3D printing. This optimization process can compromise the accuracy of the reproduced structures, emphasizing the need for further advancements in 3D printing technologies.

– FDM printing is cost-effective, widely accessible, and capable of producing core clones with relatively consistent macroscopic pore distributions. It is particularly useful for creating larger pore structures and can be readily adapted for various materials. However, FDM faces significant issues, such as the presence of interlayer gaps that lead to inflated porosity and permeability values, regardless of nozzle size. The μCT analysis revealed that these gaps contribute to the overestimation of both porosity and permeability, as they introduce additional voids not present in the original digital model. Additionally, the experimental data indicate that the permeability measurements vary significantly, underscoring the challenges of using FDM for applications requiring precise control over flow properties.

– DLP printing offers higher accuracy and fidelity in replicating complex pore structures compared to FDM. It is particularly effective at reproducing smaller pore sizes, which are crucial for accurately simulating the behavior of reservoir rocks. The layer-by-layer photopolymerization process inherent to DLP is closer to natural sedimentation processes, potentially making it a more suitable technique for creating geological models. Despite its higher precision, DLP printing faces challenges such as the retention of uncured photopolymer resin within the pore structures, which cannot be fully removed through simple solvent filtration. This residual resin alters the porosity and permeability of the printed samples, affecting their suitability for accurate geological modeling. Additionally, the formation of cracks during the curing process due to internal stresses is another significant drawback that must be addressed.

– The results of the study show that both FDM and DLP methods encounter challenges in the reproducibility of pore structures, particularly when it comes to fine details. In FDM printing using a 0.2 mm nozzle, the surface pore distribution and sizes across multiple 3D-printed clones appear similar. However, a closer examination of the μCT slices reveals inconsistencies in the replication of smaller pores. While larger pores are generally consistent, smaller pores are frequently absent in some clones but present in others. This suggests that minor variations in the printing process can lead to discrepancies in pore replication, even when using the same G-code. Similarly, in DLP printing, despite achieving better accuracy in preserving the morphology of large pores, the method also struggles with reproducing small pore elements. Even though DLP maintains the overall structure of larger pores, smaller pores are often missing or incomplete.

– To advance the application of 3D printing in replicating reservoir core plugs, several challenges must be addressed:

a) Resolution enhancement: further improvements in printing resolution are essential to bridge the gap between current 3D printing capabilities and the fine-scale features of reservoir rocks.

b) Material optimization: developing new materials with properties more closely aligned with those of reservoir rocks could improve the accuracy of the printed models.

c) Process optimization: refining the printing and curing processes to reduce defects, such as cracks in DLP prints, will enhance the reliability and applicability of these techniques in geological modeling.

d) Data processing: advanced algorithms for optimizing μCT data, including more accurate methods for surface smoothing and pore structure expansion, will help preserve the integrity of complex pore morphologies during 3D printing.

Acknowledgements

This work was funded by the subsidy allocated to Kazan Federal University for the state assignment in the sphere of scientific activities, project № FZSM-2023-0014.

References

1. Kadyrov R.I. et al. Structural Transformation of the Void-Pore Space of a Lime Reservoir During HCl Treatment // Chem. Technol. Fuels Oils. 2018. Vol. 54, № 3. P. 307–318.

2. Kadyrov R., Statsenko E., Galiullin B. The porous space structure of domanik shales in the east of Russian plate // International Multidisciplinary Scientific GeoConference Surveying Geology and Mining Ecology Management, SGEM. International Multidisciplinary Scientific Geoconference, 2018. Vol. 18, № 1.4. P. 907–914 (10.5593/sgem2018/1.4/S06.118) (https://sgemworld.at/sgemlib/spip.php?article12347).

3. McPhee C., Reed J., Zubizarreta I. Core Analysis: A Best Practice Guide (Developments in Petroleum Science): Volume 64. 1st Editio. Elsevier Science Ltd, 2015. 852 p.

4. Physics of Petroleum Reservoirs / ed. Hu X. et al. Berlin, Heidelberg: Springer Berlin Heidelberg, 2017.

5. Gaafar G.R., Tewari R.D., Zain Z.M. Overview of Advancement in Core Analysis and Its Importance in Reservoir Characterisation for Maximising Recovery. 2015. Vol. Day 1 Tue,. P. D011S003R009.
6. Cruz-Maya J.A. et al. Three-Dimensional Printing of Synthetic Core Plugs as an Alternative to Natural Core Plugs: Experimental and Numerical Study // Processes. 2023. Vol. 11, № 9. P. 2530.
7. Almetwally A.G., Jabbari H. Experimental investigation of 3D printed rock samples replicas // J. Nat. Gas Sci. Eng. 2020. Vol. 76. P. 103192.
8. Almetwally A.G., Jabbari H. 3D-Printing Replication of Porous Media for Lab-Scale Characterization Research // ACS Omega. American Chemical Society, 2021. Vol. 6, № 4. P. 2655–2664.
9. Wajahat M. et al. A review on extrusion-based 3D-printed nanogenerators for energy harvesting // J. Mater. Sci. 2022. Vol. 57, № 1. P. 140–169.
10. Ishutov S. et al. 3D printing sandstone porosity models // Interpretation. Society of Exploration Geophysicists, 2015. Vol. 3, № 3. P. SX49–SX61.
11. Ishutov S. et al. Replication of Carbonate Reservoir Pores at the Original Size Using 3D Printing // Petrophysics – SPWLA J. Form. Eval. Reserv. Descr. 2021. Vol. 62, № 5. P. 477–485.
12. Ma S. et al. 3D Printed Rocks - An Emerging Technology for Systematic Petrophysical Studies // Day 2 Mon, February 20, 2023. SPE, 2023.
13. Mukhametrakhimov R. et al. Structure of 3D-Printed Concrete by X-ray Computed Tomography // Lecture Notes in Civil Engineering. Springer International Publishing Cham, 2023. Vol. 291. P. 425–436.
14. Kong L. et al. 3D Printing for Experiments in Petrophysics, Rock Physics, and Rock Mechanics: A Review // SPE Reserv. Eval. Eng. 2021. Vol. 24, № 04. P. 721–732.
15. Almetwally A.G., Jabbari H. Experimental investigation of 3D printed rock samples replicas // J. Nat. Gas Sci. Eng. 2020. Vol. 76. P. 103192.
16. Song R. et al. 3D Printing of natural sandstone at pore scale and comparative analysis on micro-structure and single/two-phase flow properties // Energy. 2022. Vol. 261. P. 125226.
17. Wang X. et al. Effect of Porosity on Mechanical Properties of 3D Printed Polymers: Experiments and Micromechanical Modeling Based on X-ray Computed Tomography Analysis // Polymers (Basel). 2019. Vol. 11, № 7. P. 1154.
18. Goral J., Deo M. Nanofabrication of synthetic nanoporous geomaterials: from nanoscale-resolution 3D imaging to nano-3D-printed digital (shale) rock // Sci. Rep. 2020. Vol. 10, № 1. P. 21596.
19. Cruz-Maya J.A. et al. Three-Dimensional Additive Manufacturing of Artificial Oil Reservoir Rock Core Plugs for Core Flooding Experimental Tests // 3D Print. Addit. Manuf. 2022. Vol. 9, № 4. P. 233–244.
20. Stoporev A. et al. Three-Dimensional-Printed Polymeric Cores for Methane Hydrate Enhanced Growth // Polymers (Basel). 2023. Vol. 15, № 10.
21. Li H. et al. Empowering microfluidics by micro-3D printing and solution-based mineral coating // Soft Matter. 2020. Vol. 16, № 29. P. 6841–6849.
22. Wang Y. et al. Design and fabrication of rock-based microfluidics by 3D printing: the structure characterization and pore-scale flow experiment validation // J. Porous Media. 2021. Vol. 24, № 12. P. 77–92.
23. Phoenix V|tome|x S240 [Electronic resource]. URL: https://www.bakerhughes.com/waygate-technologies/industrial-radiography-and-ct/ct-inspection-systems/vtomex-s (accessed: 05.01.2025).
24. Phoenix datos|x - CT Data Acquisition Software [Electronic resource]. URL: https://www.bakerhughes.com/waygate-technologies/ndt-software/phoenix-datosx-industrial-ct-acquisition-reconstruction-software (accessed: 05.01.2025).

25. Avizo Software [Electronic resource]. URL: https://www.thermofisher.com/de/en/home/electron-microscopy/products/software-em-3d-vis/avizo-software.html (accessed: 05.01.2025).
26. Youssef S. et al. High resolution CT and pore-network models to assess petrophysical properties of homogeneous and heterogeneous carbonates // Society of Petroleum Engineers - SPE/EAGE Reservoir Characterization and Simulation Conference 2007. Society of Petroleum Engineers, 2007. P. 280–291 (doi: 10.2523/111427-ms) (http://www.spe.org/elibrary/servlet/spepreview?id=SPE-111427-MS).
27. Meet the Pro2 Series [Electronic resource]. URL: https://www.raise3d.com/pro2-series/ (accessed: 05.01.2025).
28. ideaMaker [Electronic resource]. URL: https://www.ideamaker.io/download.html (accessed: 05.01.2025).
29. Anycubic Photon Mono X [Electronic resource]. URL: https://store.anycubic.com/products/photon-mono-x-resin-printer (accessed: 05.01.2025).
30. Anycubic Photon Workshop 3D Slicer Software [Electronic resource]. URL: https://store.anycubic.com/pages/anycubic-photon-workshop-3d-slicer-software (accessed: 05.01.2025).
31. Rock Permeability Testing System [Electronic resource]. URL: https://www.wille-geotechnik.com/en/rock/rock-permeability-test-system.html (accessed: 05.01.2025).
32. The “PIK-PP” automated device for measuring porosity and permeability [Electronic resource]. URL: https://en.geologika.ru/product/the-pik-pp-automated-device-for-measuring-porosity-and-permeability/ (accessed: 05.01.2025).